ELSEVIER

Chemical Engineering Science 61 (2006) 7593–7608

Chemical Engineering Science

www.elsevier.com/locate/ces

Numerical simulation of the dynamic flow behavior in a bubble column: A study of closures for turbulence and interface forces

D. Zhang, N.G. Deen*, J.A.M. Kuipers

University of Twente, Faculty of Science and Technology, P.O. Box 217, 7500 AE Enschede, Netherlands

Received 21 June 2006; received in revised form 22 August 2006; accepted 22 August 2006
Available online 5 September 2006

Abstract

Numerical simulations of the bubbly flow in two square cross-sectioned bubble columns were conducted with the commercial CFD package CFX-4.4. The effect of the model constant used in the sub-grid scale (SGS) model, C_S, as well as the interfacial closures for the drag, lift and virtual mass forces were investigated. Furthermore, the performance of three models [Pfleger, D., Becker, S., 2001. Modeling and simulation of the dynamic flow behavior in a bubble column. Chemical Engineering Science, 56, 1737–1747; Sato, Y., Sekoguchi, K.,1975. Liquid velocity distribution in two-phase bubble flow. International Journal of Multiphase Flow 2, 79–95; Troshko, A.A., Hassan, Y.A., 2001. A two-equation turbulence model of turbulent bubbly flows. International Journal of Multiphase Flow 27, 1965–2000] to account for the bubble-induced turbulence in the k–ε model was assessed. All simulation results were compared with experimental data for the mean and fluctuating liquid and gas velocities. It is shown that the simulation results with $C_S = 0.08$ and 0.10 agree well with the measurements. When C_S is increased, the effective viscosity increases and subsequently the bubble plume becomes less dynamic. All three bubble-induced turbulence models could produce good solutions for the time-averaged velocity. The models of Troshko and Hassan and Pfleger and Becker reproduce the dynamics of the bubbly flow in a more accurate way than the model of Sato and Sekoguchi. Based on the comparison of the results obtained for two columns with different aspect ratio ($H/D = 3$ and $H/D = 6$), it was found that the model of Pfleger and Becker performs better than the model of Troshko and Hassan, while the model of Sato and Sekoguchi performs the worst. It was observed that the interfacial closure model proposed by Tomiyama [2004. Drag, lift and virtual mass forces acting on a single bubble. Third International Symposium on Two-Phase Flow Modeling and Experimentation, Pisa, Italy, 22–24 September] performs better for the taller column. With the drag coefficient proposed by Tomiyama, the predicted slip velocity agrees well with the experimental data in both columns. The virtual mass force has a small influence on the investigated bubbly flow characteristics. However, the lift force strongly influences the bubble plume dynamics and consequently determines the shape of the vertical velocity profile. In a taller column, the lift coefficient following from the model of Tomiyama produces the best results.
© 2006 Elsevier Ltd. All rights reserved.

Keywords: Bubble column; Bubbly flow; Bubble-induced turbulence; Euler–Euler model; Interfacial closures; k–ε model; Sub-grid scale model

1. Introduction

Bubble column reactors are widely used in chemical, petrochemical and biochemical processes. The ability to predict fluid dynamics is of paramount importance in designing and developing bubble column reactors. Experimental investigations and numerical simulations are widely used to study gas–liquid flow in detail.

Numerical simulation of multiphase flows has made significant progress in the last two decades. Two approaches are mostly used to simulate the flow in bubble columns: the Euler–Euler (E–E) approach (Pan et al., 1999; Sokolichin and Eigenberger, 1999; Torvik and Svendsen, 1990) and the Euler–Lagrange (E–L) approach (Delnoij et al., 1997; Van den Hengel et al., 2005; Darmana et al., 2005, 2006). Both approaches have their advantages and disadvantages and their specific range of applicability. In the Euler–Lagrange approach, each bubble is separately tracked while the liquid phase is treated as a continuum. Furthermore, the interaction between the bubbles leading to coalescence and break-up

* Corresponding author. Tel.: +31 53 489 4138; fax: +31 53 489 2882.
E-mail address: N.G.Deen@utwente.nl (N.G. Deen).

0009-2509/$ - see front matter © 2006 Elsevier Ltd. All rights reserved.
doi:10.1016/j.ces.2006.08.053

can be modeled straightforwardly. The interaction between the bubbles and the liquid is accounted for through a source term in the momentum equations. In the Euler–Euler approach, which is also referred to as the two-fluid model, both phases are treated as interpenetrating fluids. The ensemble-averaged mass and momentum conservation equations are used to describe the time-dependent motion of both phases. Ensemble-averaged interaction terms describing the effects of drag, virtual mass and lift forces appear in the momentum balances of both phases. Contrary to the Lagrangian approach, no individual bubbles are considered. The advantage of the Eulerian approach with respect to the Lagrangian approach is experienced when the void fraction of the dispersed phase is high as more bubbles need to be tracked in the Lagrangian approach, requiring additional computational time.

Turbulence modeling is one of the main unresolved problems in the simulation of gas–liquid two-phase flow. Zero equation turbulence models have been used (Pan et al., 1999), as well as the k–ε model (Becker et al., 1994; Viollet and Simonin, 1994; Pfleger and Becker, 2001; Borchers et al. (1999)) and sub-grid scale (SGS) models (Deen et al., 2001; Milelli et al., 2001; Lakehal et al., 2002). Through a detailed study of the k–ε and sub-grid scale (SGS) models used for the simulation of bubbly flow, Deen (2001) found that, although good agreement was obtained with the k–ε model in the simulation of the bubbly flow in a pseudo 2D column (i.e., the 'Becker case', Becker et al., 1994), the simulation of a three-dimensional bubble column requires the use of a SGS model to obtain quantitative agreement with experimental data. Deen et al. (2001) used a fixed value for the model constant appearing in the SGS Smagorinksky model (Smagorinsky, 1963), C_S, based on single-phase flow conditions. However, the sensitivity of the model results with respect to this model constant is not clear.

When the k–ε model is employed to evaluate the shear-induced turbulent viscosity, the bubble-induced turbulence is generally accounted for through two different approaches: Sato and Sekoguchi (1975) directly added an extra term to the effective viscosity, whereas in the other approach, the turbulence induced by the bubbles is accounted for by source terms appearing in the equations of k and ε (Mudde and Simonin, 1999; Pfleger and Becker, 2001; Troshko and Hassan, 2001). There exist several models for the source terms due to bubble-induced turbulence (Bel F'dhila and Simonin, 1992; Gosman et al., 1992; Kataoka and Serizawa, 1989; Lopez de Bertodano et al., 1994; Pfleger and Becker, 2001; Troshko and Hassan, 2001). In the model of Gosman et al. (1992), these terms in the equation for the liquid turbulent kinetic energy, k originates from the gas fluctuation and dispersion, whereas the bubble-induced production term in the equation for the liquid turbulence dissipation rate, ε, comes from the gas dissipation rate. In other models (Kataoka and Serizawa, 1989; Pfleger and Becker, 2001; Troshko and Hassan, 2001), the production of bubble-induced turbulent kinetic energy is calculated as the work of the bubble, i.e., the interfacial force multiplied with the local slip velocity. In this case, the associated energy dissipation rate is scaled with a time scale, τ_{BIT}. Oey et al. (2003) found that in the simulation of the Becker case (Becker et al., 1994), the model of Gosman et al. (1992) and that of Bel F'dhila and Simonin (1992) do not yield a large difference in the global column dynamics. The main difference among the bubble-induced turbulence models of Pfleger and Becker (2001) and Troshko and Hassan (2001) lies in the time scale of the bubble-induced turbulence dissipation. In the model of Pfleger and Becker (2001), the smallest eddy time scale of the shear-induced turbulence was used as the characteristic time scale of the bubble-induced turbulence. Lopez de Bertodano (1992) found that when the shear-induced turbulence time scale is used as an estimate for the time scale ofthe bubble-induced turbulence, the turbulence decay depends on the initial dissipation rate, which is unphysical. For this reason he proposed a new expression for the bubble-induced turbulence time scale, which depends on the bubble relaxation time. Troshko and Hassan (2001) also adopted this time scale. In the simulations of Pfleger and Becker (2001) and Troshko and Hassan (2001), numerical results fit well with the experiments, though the time scale used to calculate the bubble-induced turbulence production in the liquid phase turbulence dissipation rate equation are quite different. Although all these models can provide good solutions for the time-averaged velocities, to the best of our knowledge, neither the validity of the predicted sub-grid scale quantities, nor the difference between these models has been investigated systematically before. In this work, the performance of these two models, along with the model of Sato and Sekoguchi (1975) was investigated for the case of a square cross-sectioned bubble column.

A correct description of the closure laws for the drag, lift and virtual mass forces is of great importance in numerical simulation of bubbly flows. Despite considerable research efforts on this topic (Clift et al., 1978; Ervin and Tryggvason, 1997; Magnaudet and Eames, 2000; Tomiyama et al., 2002), accurate modeling of the interfacial forces remains an open question in numerical simulations of bubbly flow. For a single bubble, its shape varies with the bubble size, continuous phase flow field, and the physical properties of the system, which turns the interfacial force closures into a complex function of the bubble Reynolds number (Re), the Eötvös number (Eo), and the Morton number (M). Consequently, different drag correlations (Clift et al., 1978; Ishii and Zuber, 1979; Tomiyama, 1998; Tomiyama et al., 2002) and lift coefficients (Svendsen et al., 1992; Tomiyama et al., 1995, 2002) are found in literature. Recently, Tomiyama (2004) proposed a set of closures for the drag, lift and virtual mass forces based on a large body of experimental data. However, the performance of these closures in bubbly flow simulations has not been reported so far.

In this work we present three-dimensional dynamic simulations of gas–liquid bubbly flow, employing the Euler–Euler approach for the case of square cross-sectioned bubble columns of two different aspect ratios. The sensitivity of the sub-grid scale model to the model constant C_S and the applicability of three different bubble-induced turbulence models proposed by Sato and Sekoguchi (1975), Pfleger and Becker (2001) and Troshko and Hassan (2001) are investigated in detail. Furthermore, the performance and applicability of the interfacial force closures proposed by Tomiyama (2004) as well as the effect of the drag, lift and

virtual mass forces are studied. All the numerical results are compared with experimental measurement data of Deen et al. (2001).

2. Governing equations

The equations of the two-fluid model are derived by ensemble-averaging the local instantaneous equations for single-phase flow (Drew and Passman, 1999). Two sets of balance equations for mass and momentum are obtained. Ignoring the interfacial mass transfer, the generic conservation equations for mass and momentum respectively take the following form:

$$\frac{\partial(\alpha_k\rho_k)}{\partial t} + \nabla\cdot(\alpha_k\mathbf{U}_k) = 0, \tag{1}$$

$$\frac{\partial(\alpha_k\rho_k\mathbf{U}_k)}{\partial t} + \nabla\cdot(\alpha_k\rho_k\mathbf{U}_k\mathbf{U}_k + \alpha_k\tau_k) = \alpha_k\rho_k\mathbf{g} - \alpha_k\nabla p_k + \mathbf{M}_k, \tag{2}$$

where the indices k refers to the phase (L for liquid, G for gas). $\mathbf{U} = (u, v, w)$ is the velocity of phase k. The volume fraction of each phase is denoted by α. For phase k, the stress tensor τ_k reads

$$\tau_k = -\mu_{\text{eff}}(\nabla\mathbf{U}_k + (\nabla\mathbf{U}_k)^{\mathrm{T}} - \tfrac{2}{3}I\nabla\cdot\mathbf{U}_k), \tag{3}$$

where the liquid phase effective viscosity, $\mu_{L,\text{eff}}$, is composed of three contributions: the molecular viscosity $\mu_{L,L}$, the shear-induced turbulent viscosity $\mu_{L,\text{Tur}}$, and an optional term due to bubble-induced turbulence μ_{BIT}:

$$\mu_{L,\text{eff}} = \mu_{L,L} + \mu_{L,\text{Tur}} + \mu_{BIT}. \tag{4}$$

In this work, both the sub-grid model (SGS) proposed by Smagorinsky (1963) and the k–ε turbulence models were employed to evaluate the shear-induced turbulent viscosity in the liquid phase. Turbulence in the gas phase is ignored but the gas phase influences the turbulence in the liquid phase through a model for the bubble-induced turbulence.

When the SGS turbulence model is employed, the liquid phase shear-induced turbulent viscosity is modeled through the following equation:

$$\mu_{L,\text{Tur}} = \rho_L(C_S\Delta)^2|\mathbf{S}|, \tag{5}$$

where $\mathbf{S}$ is the characteristic filtered rate of strain and $\Delta = (\Delta_i\Delta_j\Delta_k)^{1/3}$ is the filter width. C_S is a dimensionless model constant, which typically ranges between 0.08 and 0.22 for single-phase flows (Canuto and Cheng, 1997).

The gas phase effective viscosity was calculated following Jakobsen et al. (1997):

$$\mu_{G,\text{eff}} = \frac{\rho_G}{\rho_L}\mu_{L,\text{eff}}. \tag{6}$$

When the k–ε model is used, the shear-induced turbulent viscosity in the liquid phase is formulated as follows:

$$\mu_{L,\text{Tur}} = C_\mu\rho_L\frac{k_L^2}{\varepsilon_L}. \tag{7}$$

The conservation equations for k and ε are, respectively, given by

$$\frac{\partial(\alpha_L\rho_Lk_L)}{\partial t} + \nabla\cdot\left(\alpha_L\rho_L\mathbf{U}_Lk_L - \alpha_L\left(\mu_{L,L}+\frac{\mu_{L,\text{Tur}}}{\sigma_k}\right)\nabla k_L\right) = \alpha_L(G_L - \rho_L\varepsilon_L) + S_{k,BIT}, \tag{8}$$

$$\frac{\partial(\alpha_L\rho_L\varepsilon_L)}{\partial t} + \nabla\cdot\left(\alpha_L\rho_L\mathbf{U}_L\varepsilon_L - \alpha_L\left(\mu_{L,L}+\frac{\mu_{L,\text{Tur}}}{\sigma_\varepsilon}\right)\nabla\varepsilon_L\right) = \frac{\alpha_L\varepsilon_L}{k_L}(C_{\varepsilon1}G_L - C_{\varepsilon2}\rho_L\varepsilon_L) + S_{\varepsilon,BIT} \tag{9}$$

with $C_k = 1.44$, $C_{\varepsilon1} = 1.44$, $C_{\varepsilon2} = 1.92$, $C_\varepsilon = 1.92$, $C_\mu = 0.09$, $\sigma_k = 1.0$ and $\sigma_\varepsilon = 1.217$. It is noted that these constants are not universal, even in the case of single-phase flow. For multiphase flows they are still under debate. $S_{k,BIT}$ and $S_{\varepsilon,BIT}$ are source terms due to presence bubbles, which will be discussed in detail later.

The velocity fluctuations induced by displacement of the liquid as the bubbles pass by is often referred to as pseudo-turbulence or bubble-induced turbulence. When the SGS turbulence model is used to evaluate the shear-induced turbulent viscosity, the model proposed by Sato and Sekoguchi (1975) is adopted to account for the bubble-induced turbulence in Eq. (4):

$$\mu_{BIT} = \rho_L\alpha_GC_{\mu,BIT}d_B|\mathbf{U}_G - \mathbf{U}_L|. \tag{10}$$

When the k–ε turbulence model is used to evaluate the shear-induced turbulent viscosity, there are two approaches to account for the bubble-induced turbulence. One is to use the standard k–ε model, i.e., $S_{k,BIT}$ and $S_{\varepsilon,BIT}$ in Eqs. (8) and (9) are set to zero, while the bubble-induced turbulence is accounted for through Eq. (10). Another approach to account for the bubble-induced turbulence is to include extra source terms in the turbulence models, that is, the bubble-induced turbulence is implicitly included in Eq. (7), and μ_{BIT} is set to zero in Eq. (4). As mentioned earlier, the source terms proposed by Pfleger and Becker (2001) and Troshko and Hassan (2001) were selected to account for the bubble-induced turbulence. All three bubble-induced turbulence models used in the k–ε model are summarized in Table 1.

In the approach of Pfleger and Becker (2001), $|\mathbf{M}_L|.|\mathbf{U}_G - \mathbf{U}_L|$ represents the rate of energy input of the bubbles resulting from the interfacial forces and the slip velocity. $\tau_{BIT} = \varepsilon_L/k_L$ represents the time scale for the dissipation of the bubble-induced turbulence. In the approach of Troshko and Hassan (2001), only the drag force is considered in the energy input of the bubbles; the characteristic time-scale of bubble-induced turbulence is set equal to the bubble response time, $\tau_{BIT} = 2C_{VM}d_B/(3C_D|\mathbf{U}_G - \mathbf{U}_L|)$. It is noted that the drag is the main source of energy input. Consequently the difference between the models is mainly expressed through the characteristic time scale of the bubble-induced turbulence.

The term $\mathbf{M}_k$ in Eq. (2), describes the interfacial forces and is given as follows:

$$\mathbf{M}_L = -\mathbf{M}_G = \mathbf{M}_{D,L} + \mathbf{M}_{L,L} + \mathbf{M}_{VM,L}, \tag{11}$$

where the terms on the right-hand side represent forces due to drag, lift and virtual mass, respectively. These are calculated

Table 1
Three different models for bubble-induced turbulence in bubbly flow

BIT model	Source		μ_{BIT}
	$S_{k,BIT}$	$S_{\varepsilon,BIT}$	
1 (Sato and Sekoguchi, 1975)	0	0	Eq. (9)
2 (Pfleger and Becker, 2001)	$\alpha_L C_k \lvert\mathbf{M}_L\rvert\lvert\mathbf{U}_G - \mathbf{U}_L\rvert$	$\frac{\varepsilon_L}{k_L} C_\varepsilon S_{k,BIT}$	0
3 (Troshko and Hassan, 2001)	$\lvert\mathbf{M}_{D,L}\rvert\lvert\mathbf{U}_G - \mathbf{U}_L\rvert$	$0.45\frac{3C_D\lvert\mathbf{U}_G - \mathbf{U}_L\rvert}{2C_{VM}d_B} S_{k,BIT}$	0

Table 2
Investigated interfacial force closures

Closure model A	Closure model B (Tomiyama, 2004)
$C_D = \frac{2}{3}\sqrt{Eo}$ (Ishii–Zuber, 1979)	$C_D = \frac{8}{3}\frac{Eo(1-E^2)}{E^{2/3}Eo + 16(1-E^2)E^{4/3}} F(E)^{-2}$ $E = \frac{1}{1+0.163Eo^{0.757}}$ (Wellek et al., 1966) $F(E) = \frac{\sin^{-1}\sqrt{1-E^2} - E\sqrt{1-E^2}}{1-E^2}$
$C_L = 0.5$	$C_L = \begin{cases} \min[0.288\tanh(0.121\,\mathrm{Re}),\, f(Eo_d)] & Eo_d < 4, \\ \lvert f(Eo_d) & Eo_d \geqslant 4 \end{cases}$ $Eo_d = Eo/E^{2/3}$ $f(Eo_d) = 0.00105Eo_d^3 - 0.0159Eo_d^2 - 0.0204Eo_d + 0.474$
$C_{VM,h} = 0.5$	$C_{VM,h} = \frac{E\cos^{-1}E - \sqrt{1-E^2}}{E^2\sqrt{1-E^2} - E\cos^{-1}E}$
$C_{VM,v} = 0.5$	$C_{VM,v} = \frac{\cos^{-1}E - E\sqrt{1-E^2}}{(2E^{-1} - E)\sqrt{1-E^2} - \cos^{-1}E}$

from the following expressions:

$$\mathbf{M}_{D,L} = \frac{3}{4}\alpha_G\rho_L\frac{C_D}{d_B}\lvert(\mathbf{U}_G - \mathbf{U}_L)\rvert(\mathbf{U}_G - \mathbf{U}_L), \tag{12}$$

$$\mathbf{M}_{L,L} = \alpha_G\rho_L C_L(\mathbf{U}_G - \mathbf{U}_L) \times \nabla \times \mathbf{U}_L, \tag{13}$$

$$\mathbf{M}_{VM,L} = \alpha_G\rho_L\mathbf{C}_{VM} \cdot \left(\frac{D_G\mathbf{U}_G}{Dt} - \frac{D_L\mathbf{U}_L}{Dt}\right). \tag{14}$$

The virtual mass coefficient C_{VM} for a spherical bubble in potential flow and in a Stokes flow is known to be 0.5 in all three co-ordinate directions. According to Tomiyama (2004), for ellipsoidal bubbles the scalar C_{VM} should be replaced by a tensor, $\mathbf{C}_{VM}$ containing non-zero values on the diagonal, representing the different virtual mass coefficients in the horizontal ($C_{VM,h}$) and vertical ($C_{VM,v}$) directions.

In this paper, two sets of interfacial force closures are used. Both of these closure models are listed in Table 2.

In all simulations, a pressure boundary was applied at the outlet. No-slip conditions were used for both phases at all walls. The total domain was subdivided into uniform computational grid cells with $\Delta x = \Delta y = \Delta z = 0.01$ m. Eqs. (1) and (2) were solved in a transient fashion with a time step of 0.005 s. The curvature compensated convective transport (CCCT) scheme was used for the discretization of all convective terms. Standard boundary conditions employing wall functions were used for k and ε. Numerical simulations were conducted with the commercial CFD package CFX-4.4 of AEA Technology, Harwell, UK. The results of the numerical simulations were compared with experimental data of Deen et al. (2001). Prior to the parameter study, the grid dependency of the simulations was tested and it was found that the differences between the results from the aforementioned numerical grid and a simulation with a grid refinement of a factor of two in all directions yielded quantitatively grid independent results. That is to say that the differences in the time-averaged quantities are within about 5%.

3. Physical problem

The bubble column studied in this paper is schematically shown in Fig. 1. The entire column is initially filled with water, which acts as the continuous liquid phase. Air is used as the dispersed gas phase and injected in the center of the bottom plane with A_{in}=0.03×0.03 m^2 and $V_{G,\mathrm{in}}$=0.1225 m/s corresponding to a superficial gas velocity of 4.9 mm/s. The gas–liquid flow is assumed to be homogeneous (bubbly) flow and break-up and coalescence are not accounted for. The width, depth and height of the column are, respectively, set to $W = 0.15$ m, $D = 0.15$ m, and $H = 0.45$ m or $H = 0.90$ m. The gas distributor is situated

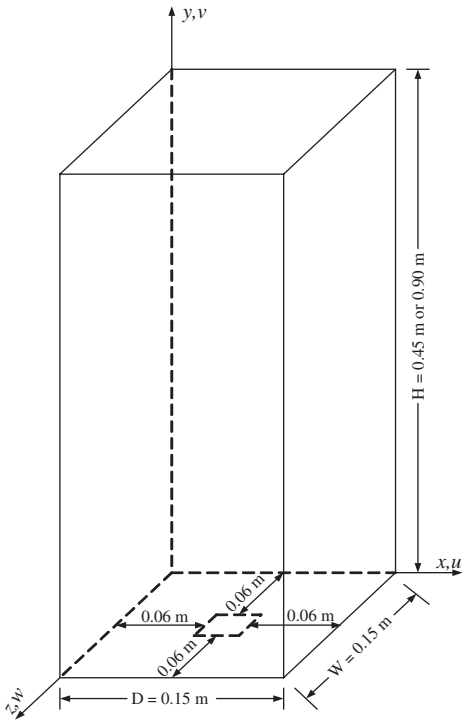

Fig. 1. Schematic representation of the investigated bubble columns.

in the bottom plane of the column at a distance of 0.06 m from each of the surrounding walls of the column. All the simulation parameters and physical properties are presented in Tables 3 and 4, where for each case the first number indicates the bubble-induced turbulence model, the capital letter refers to the interfacial closure model, the second number represents the aspect ratio of the column and an additional code indicates a specific variation (i.e., case 1B3 refers to BIT model 1, interfacial closure model **B** and $H/D=3$). The bubble size of 4 mm used in the paper of Deen et al. (2001) is based on camera observations. To get more accurate information on the bubble size we performed bubble size measurements employing the digital image analysis technique described by Van den Hengel et al. (2005). It was found that the bubble size is indeed in the order of 4 mm.

4. Data processing

In order to compare the numerical results with the experimental data, the time-averaged quantities are calculated as defined in the following expressions. The time-averaged mean velocity at time level n is calculated as

$$\overline{u_n} = \frac{n-n_0-1}{n-n_0}\overline{u_{n-1}} + \frac{1}{n-n_0}u_n, \tag{15}$$

Table 3
Simulation and case parameters employing the SGS model

H/D	Case	C_S	$(C_{vm,h}, C_{vm,v})$	C_D	C_L
	0A3-1	0.08	(0.50, 0.50)	0.98	0.50
	0A3-2	0.15	(0.50, 0.50)	0.98	0.50
	0A3-3	0.20	(0.50, 0.50)	0.98	0.50
3	0A3	0.10	(0.50, 0.50)	0.98	0.50
	0A3-DT	0.10	(0.50, 0.50)	Tomiyama (2004)	0.50
	0A3-CLT	0.10	(0.50, 0.50)	0.98	Tomiyama (2004)
	0A3-VM0	0.10	(0.0, 0.0)	0.98	0.50
	0A3-VMT	0.10	Tomiyama (2004)	0.98	0.50
	0A6-DT	0.10	(0.50, 0.50)	Tomiyama (2004)	0.50
6	0A6	0.10	(0.50, 0.50)	0.98	0.50
	0A6-CLT	0.10	(0.50, 0.50)	0.98	Tomiyama (2004)
	0B6	0.10	Tomiyama (2004)	Tomiyama (2004)	Tomiyama (2004)

$\rho_L = 1000\,\mathrm{kg/m^3}$, $\mu_{L,L} = 0.001\,\mathrm{kg/(m\,s)}$, $\sigma = 0.07275\,\mathrm{N/m}$, $\rho_G = 1.29\,\mathrm{kg/m^3}$, $d_B = 4\,\mathrm{mm}$, $\mu_G = 1.812\times10^{-5}\,\mathrm{kg/(m\,s)}$, $Eo = 2.15$

Table 4
Simulation and case parameters employing the k–ε model

H/D	Case	BIT model	$(C_{vm,h},\ C_{vm,v})$	C_D	C_L
	1A3	Sato and Sekoguchi (1975)	(0.50, 0.50)	0.98	0.50
	2A3	Pfleger and Becker (2001)	(0.50, 0.50)	0.98	0.50
3	3A3	Troshko and Hassan (2001)	(0.50, 0.50)	0.98	0.50
	2B3	Pfleger and Becker (2001)	Tomiyama (2004)	Tomiyama (2004)	Tomiyama (2004)
	1A6	Sato and Sekoguchi (1975)	(0.50, 0.50)	0.98	0.50
	2A6	Pfleger and Becker (2001)	(0.50, 0.50)	0.98	0.50
6	3A6	Troshko and Hassan (2001)	(0.50, 0.50)	0.98	0.50
	1B6	Sato and Sekoguchi (1975)	Tomiyama (2004)	Tomiyama (2004)	Tomiyama (2004)
	2B6	Pfleger and Becker (2001)	Tomiyama (2004)	Tomiyama (2004)	Tomiyama (2004)
	3B6	Troshko and Hassan (2001)	Tomiyama (2004)	Tomiyama (2004)	Tomiyama (2004)

where the averaging is started at time step $n_0 = 7500$, corresponding to 37.50 s physical time. All simulations were carried out for $n = 10^5$ time steps corresponding to a period of 500 s.

The large-scale velocity fluctuations are calculated during the calculation as follows:

$$\overline{u_{rms,n}^2} = \overline{u_n^2} - \overline{u_n}^2. \tag{16}$$

All the presented results are time-averaged quantities, which were selected in a plane at a width of $z/W = 0.50$.

5. Results and discussion

The sensitivity of the SGS model to the models constant C_S and three different closures to account for the bubble-induced turbulence in the k–ε turbulence model (see Table 1) were assessed. Furthermore, two different interfacial closure models (see Table 2) and two different column aspect ratios were investigated. All test cases are summarized in Tables 3 and 4. The effect of model constant C_S will be discussed first, followed with the investigation of the performance and capacity of three different bubble-induced turbulence models. Subsequently, the applicability of the interfacial closures proposed by Tomiyama for bubbly flow simulations will be evaluated. Finally, the effect of the drag, lift and virtual mass forces will be assessed. Based on the physical parameters given in Table 3, the interfacial closure parameters in Table 2 keep constant values: in model **A**, $C_D = 0.98$; $C_L = 0.5$ and $C_{VM,h} = C_{VM,v} = 0.5$; whereas in model **B**, $C_D = 1.52$; $C_L \approx 0.29$; $C_{VM,h} = 0.43$, $C_{VM,v} = 0.68$.

5.1. Turbulence model

5.1.1. Effect of C_S

The sensitivity of the SGS model was tested by varying the values of C_S (0.08, 0.10, 0.15, 0.20). The corresponding test cases are Case 0A3-1, 0A3, 0A3-2 and 0A3-3. Fig. 2 shows the comparison between the experimental and predicted profiles of the mean vertical velocity of both phases. It is clear from Fig. 2 that the case where $C_S = 0.08$ and 0.10 produce the best solutions, while the case with $C_S = 0.20$ provides the worst solution. This can be attributed to the fact that, as shown in Fig. 3, with the increase of C_S, the turbulent viscosity increases as well. This makes the liquid more viscous, damping the bubble plume dynamics and hence the vertical velocity profiles become increasingly steeper. Fig. 4 shows the comparison between the experimental and simulated profiles of the liquid velocity fluctuations at two different heights. First of all, it is apparent that, the fluctuations in the horizontal direction are lower than in the vertical direction, which means that the flow is non-isotropic. It is also found that, as C_S increases, the velocity fluctuation in the horizontal direction drops because of the increase of the viscosity; meanwhile v_{rms} increases at the center and decreases towards the column walls. This is due to the fact that with higher values of C_S the bubble plume fluctuates strongly only in the center of the column.

It is noted that, as can be seen in Fig. 3, the predicted effective viscosity is not damped near the wall, which is unrealistic. This can be improved by applying damping functions, as suggested by Van Driest (1956) or by using an alternative SGS model, such as the simple model suggested by Vreman (2004). As can be seen in Fig. 4, the resolved velocity fluctuations agree well with the experimental data when the model constant C_S is 0.08 or 0.10. These results are in much better agreement than those obtained with the standard k–ε model. In the latter case, Deen (2001) found that though it provides a good solution for the time-averaged vertical velocity, the standard k–ε model together with the model of Sato and Sekoguchi (1975) accounting for the bubble-induced turbulence is not capable of resolving the velocity fluctuations and produces a quasi-steady state bubble plume behavior. In order to improve the standard model, different bubble-induced turbulence models were tested. As indicated before (see Table 1), the models of Pfleger and Becker (2001) and Troshko and Hassan (2001) will be investigated. Comparisons of the velocity fluctuations with experimental data were not given in the work of Pfleger and Becker (2001) and Troshko and Hassan (2001), so in the following

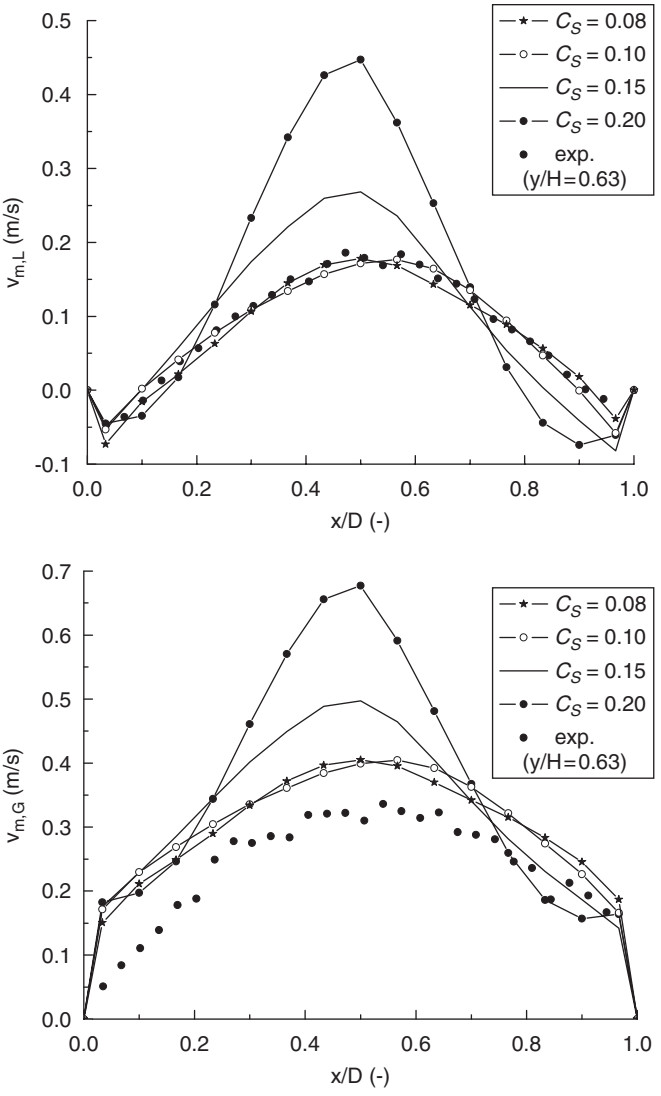

Fig. 2. Comparison of the experimental and predicted profiles of the mean vertical velocity of the both phases. The predicted profiles were obtained from different C_S values used in the SGS model.

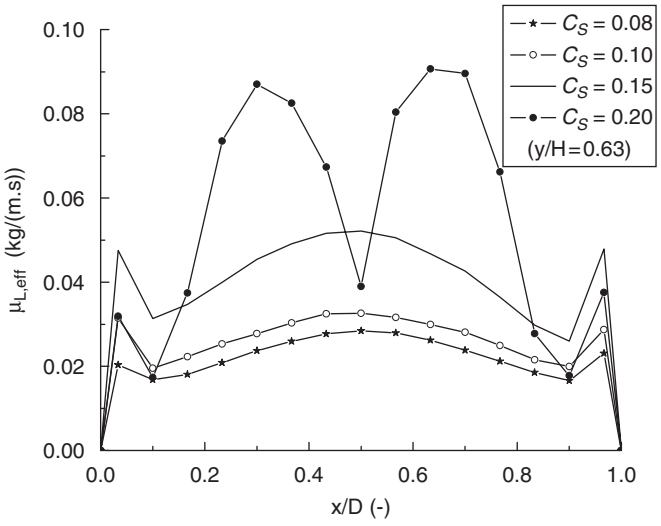

Fig. 3. Time-averaged liquid phase effective viscosity obtained from four C_S values used in the SGS model.

section the performance and capability of the three aforementioned bubble-induced turbulence models in the simulation of bubbly flow will be repeated in detail.

5.1.2. Bubble-induced turbulence model

Fig. 5 presents the time-averaged vertical velocity profiles for the cases employing different turbulence closures, i.e., cases 1A3, 2A3 and 3A3. The numerical results of case 2A3 and 3A3 slightly under-predict the experimental data for the liquid phase, but still fit reasonably well with the experimental data for the gas phase. It is clearly found in this figure that the vertical velocity profiles obtained from the model of Sato and Sekoguchi (1975) (Case 1A3) are higher than those obtained in the other two cases. This can be attributed to the higher effective viscosity predicted by the model of Sato and Sekoguchi, which is shown in Fig. 6. Comparing the bubble-induced turbulent viscosity with the local effective viscosity for Case 1A3, it is found that the bubble-induced turbulent viscosity is negligible compared to the shear-induced contribution, this means that in case 1A3 the bubble plume has hardly any influence on the liquid phase turbulence. This finding is consistent with the analysis made by Sokolichin et al. (2005). They found that the bubble-induced viscosity is almost two orders of magnitude smaller than the shear-induced part of the effective viscosity and therefore, it can hardly have any influence on the simulation results. The high eddy viscosity predicted by the k–ε model without extra source terms leads to a quasi-steady state predicted bubble plume as shown in Fig. 7, while in other cases (0A3, 2A3 and 3A3), a dynamic bubble plume is found, which is in much better agreement with the experimental observations.

In case 1A3, as the velocity fluctuations are implicitly contained in the turbulent kinetic energy k rather than captured in the standard k–ε model, the simulated velocity fluctuations underpredict the experimental data, whereas the models of Troshko and Hassan (2001) and Pfleger and Becker (2001) produce a good solution for the velocity fluctuations as shown in Fig. 8. From Figs. 7 and 8, it is found that in the simulation of

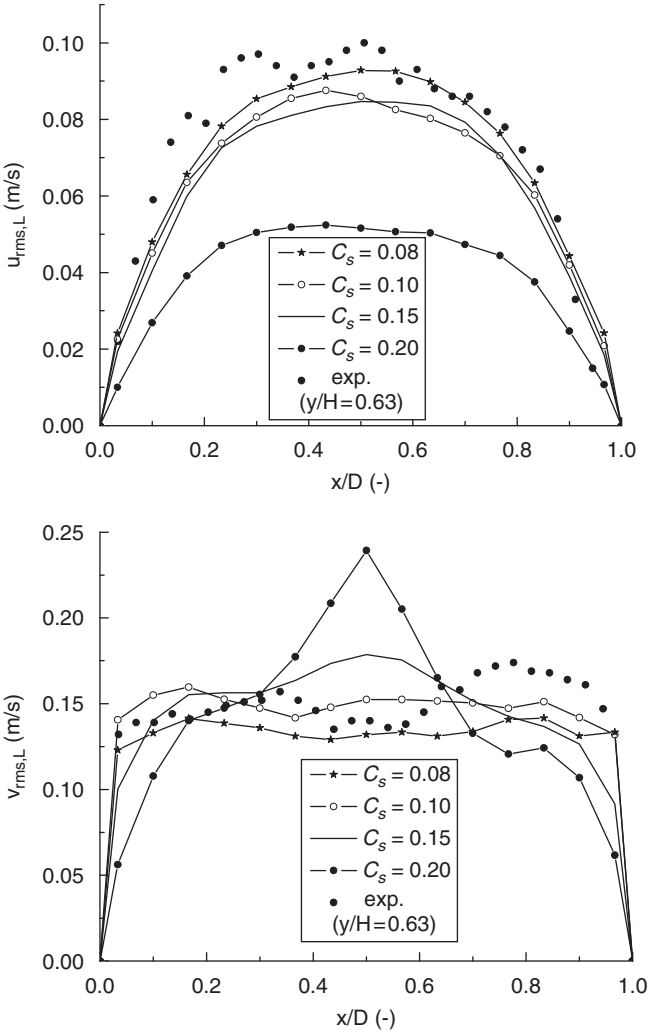

Fig. 4. Comparison of the simulated and experimental profiles of the liquid velocity fluctuations. The simulated profiles were obtained from different C_S values used in the SGS model.

bubbly flow, the k–ε model can be improved when the bubble-induced turbulence is accounted for through additional source terms as suggested by Pfleger and Becker (2001) and Troshko and Hassan (2001).

In Fig. 5, the experimental slip velocity is about 0.18 m/s, while the predicted slip velocity is about 0.23 m/s, which directly follows from the applied drag model. Based on the drag model and the related slip velocity, the time scale of the bubble-induced turbulence, according to Lopez de Bertodano (1992), $\tau_{BIT} = 2C_{VM}d_B/(3C_D|\mathbf{U}_G - \mathbf{U}_L|)$, is about 0.006 s for the studied cases (Case 0A3, 1A3, 2A3, and 3A3). This time scale is much smaller than the time scale of the smallest eddy dissipation in the liquid phase ($\tau_{SIT} = k/\varepsilon \approx 0.8$ s, Zhang et al., 2005), which means that the bubble-induced turbulence decays much faster than shear-induced turbulence in this bubbly flow. Furthermore, it is observed in Fig. 6 that the effective viscosity in Case 3A3, which mainly originates from the eddy viscosity, exhibits a local maximum near the wall, which is unphysical. Though the extra source term introduced in the ε equation in

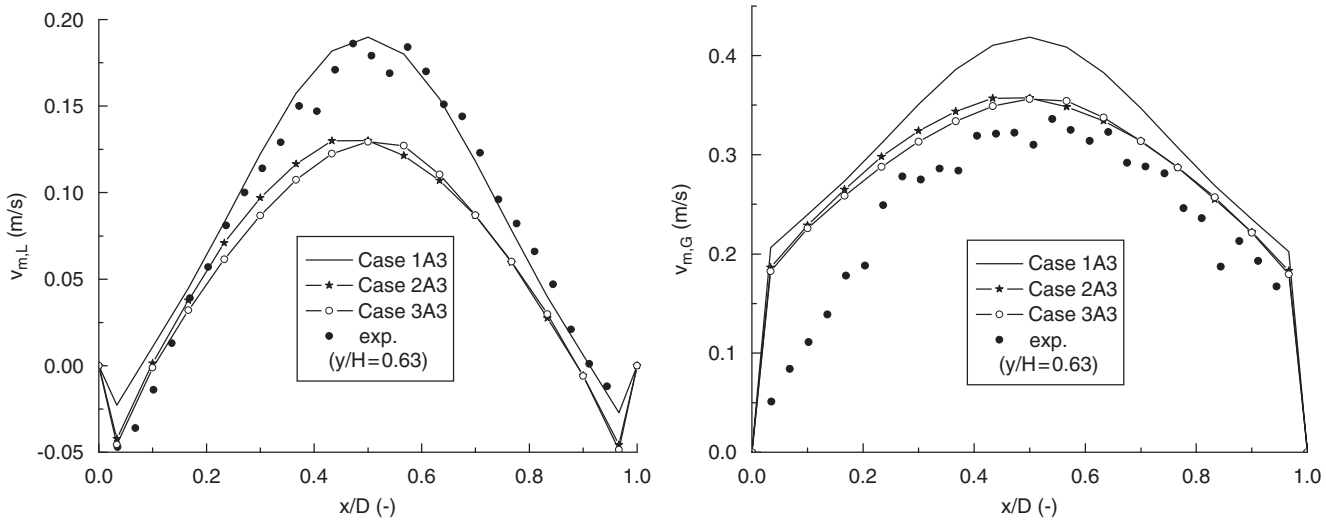

Fig. 5. Comparison of the simulated time-averaged vertical velocity profiles of both phases with the experimental data using different bubble-induced turbulence models in the k–ε model.

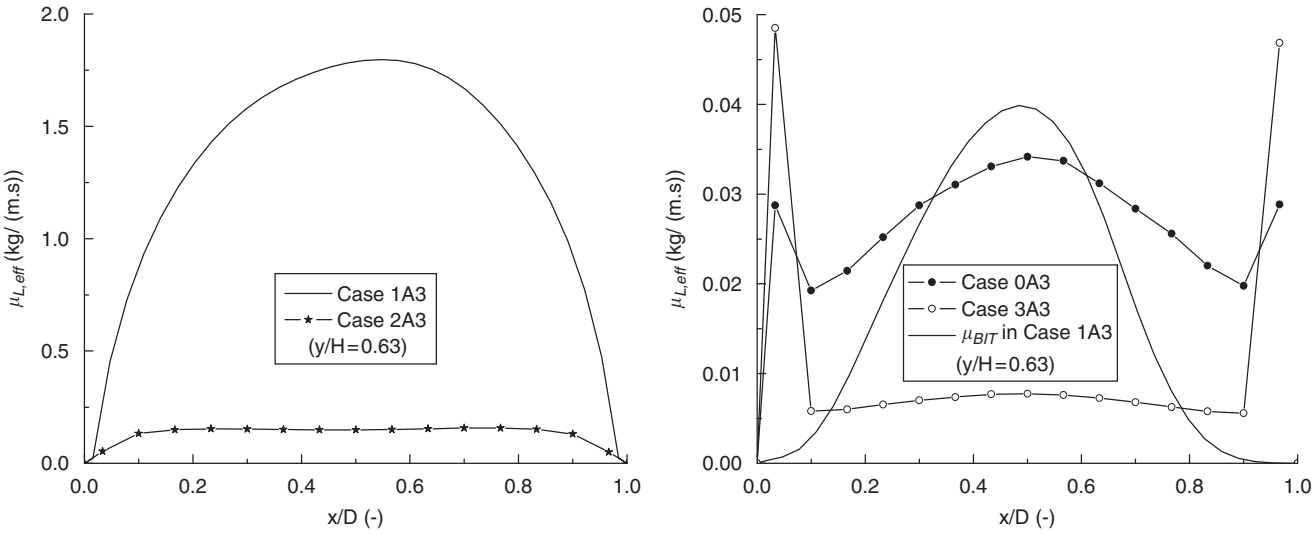

Fig. 6. Time-averaged profiles of liquid phase effective viscosity obtained from different turbulence models.

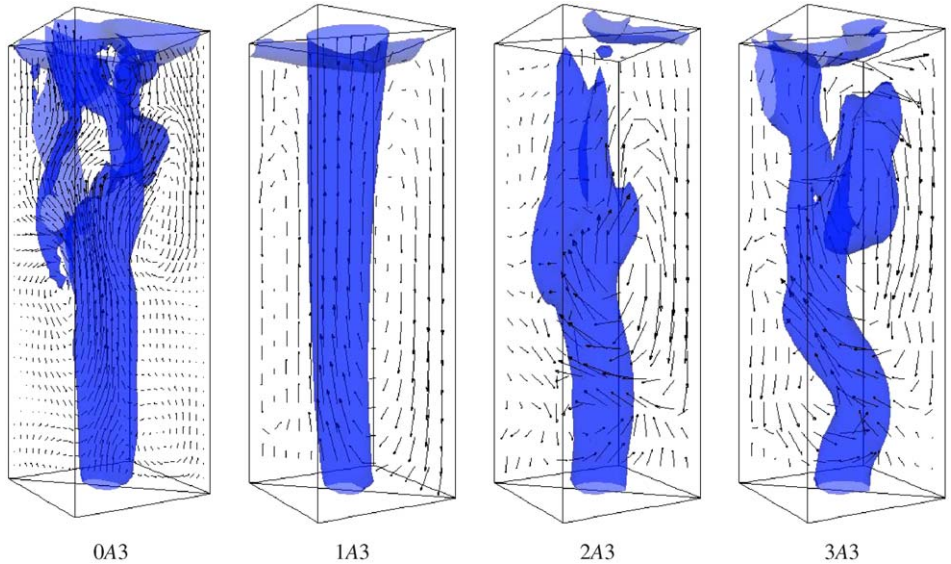

Fig. 7. Snapshots of the instantaneous iso-surfaces of $\alpha_G = 0.03$ and liquid velocity fields for different cases after 200 s.

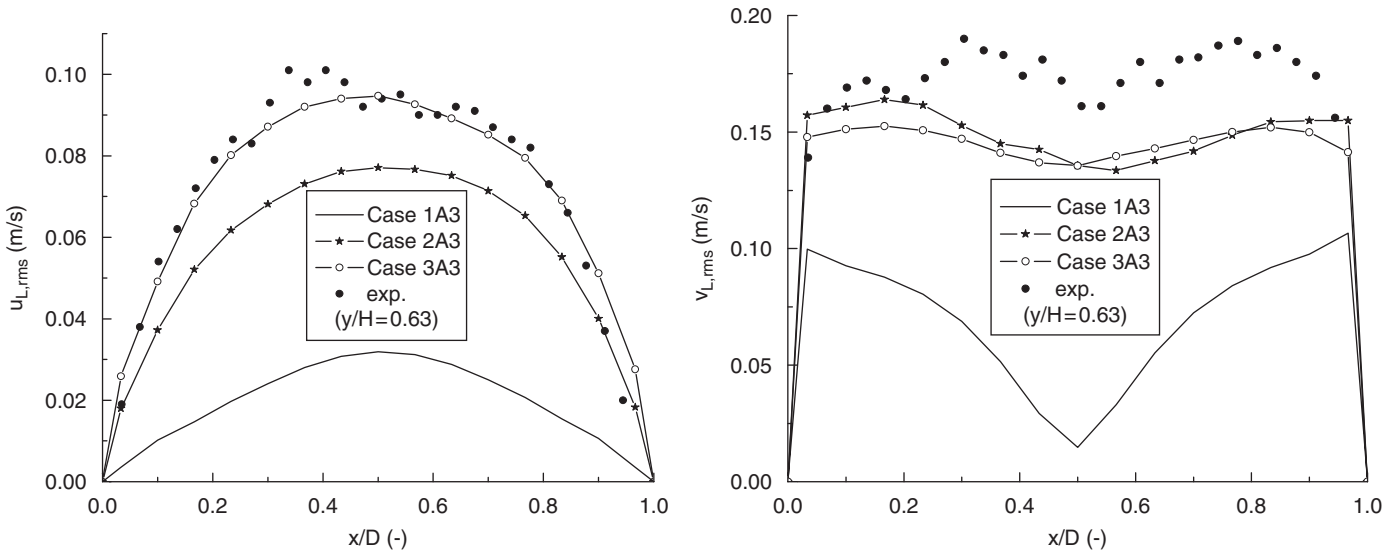

Fig. 8. Time-averaged plot of the liquid phase velocity fluctuations in horizontal and vertical directions. Different bubble-induced turbulence models together with the k–ε model are used.

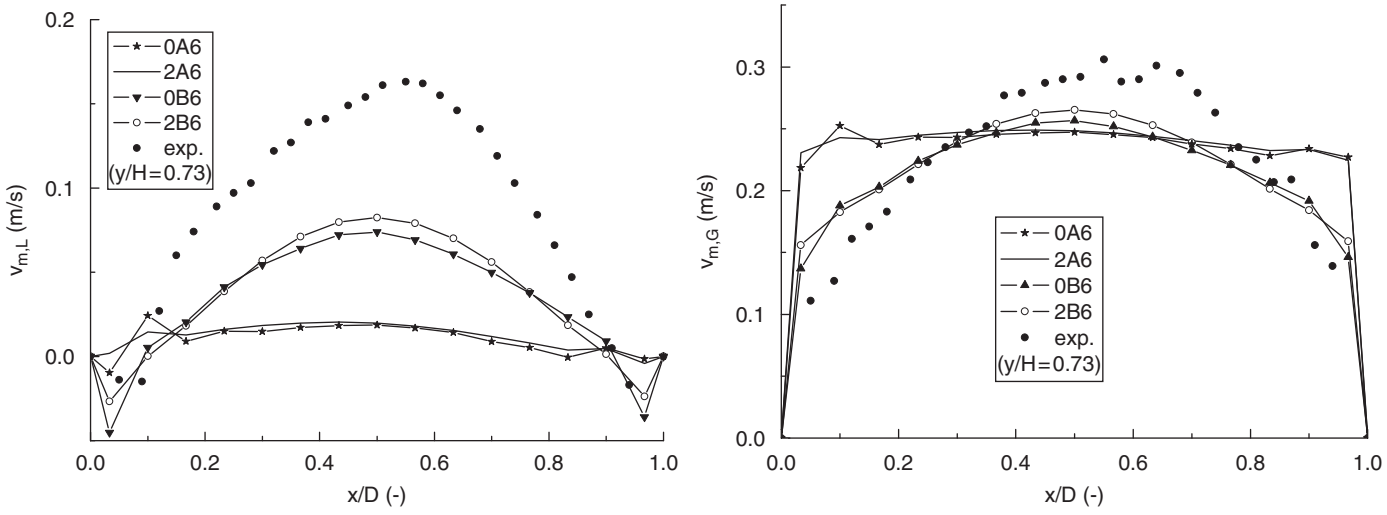

Fig. 9. Comparison of the simulated time-averaged vertical velocity profiles of both phases with the experimental data using different interfacial closures in a taller column.

case 3A3 is approximately 60 times larger than that in case 2A3, it was found earlier (Zhang et al., 2005) that both the turbulent kinetic energy k and turbulence dissipation rate ε obtained from case 3A3 are smaller than those obtained from case 2A3.

5.2. Interfacial force closures

5.2.1. Interfacial closures of Tomiyama

The interfacial closures proposed by Tomiyama (2004) were tested through cases 0A6, 0B6, 2A6 and 2B6 (see Tables 3 and 4). Fig. 9 provides the comparison of the time-averaged vertical velocity profiles for both phases in the taller column. When closure model **A** is used, relatively flatter vertical velocity profiles are predicted in the upper part of the column, which reflects that the bubble plume is spread out to the total cross-sectional area of the column and consequently a uniform velocity profile is obtained. When interfacial closure model **B** proposed by Tomiyama was adopted (Cases 0B6 and 2B6), though the liquid phase vertical velocity was under-predicted, the simulated gas phase vertical velocity distribution agrees well with the experimental data. The under-prediction of the liquid vertical velocity may come from the drag correlation or the experimental error as the experimentally measured slip velocity (0.13 m/s) is smaller than the predicted slip velocity (0.18 m/s). Contrary to the results of model **A**, the vertical velocity profiles obtained from Tomiyama's interfacial closures are not flat, which can be attributed to the lift force. In Tomiyama's model **B**, the value of C_L is relatively small ($C_L \approx 0.29$) compared to that in case **A** ($C_L = 0.5$). Consequently, the bubble plume is dispersed less, which leads to a relatively steep velocity profile.

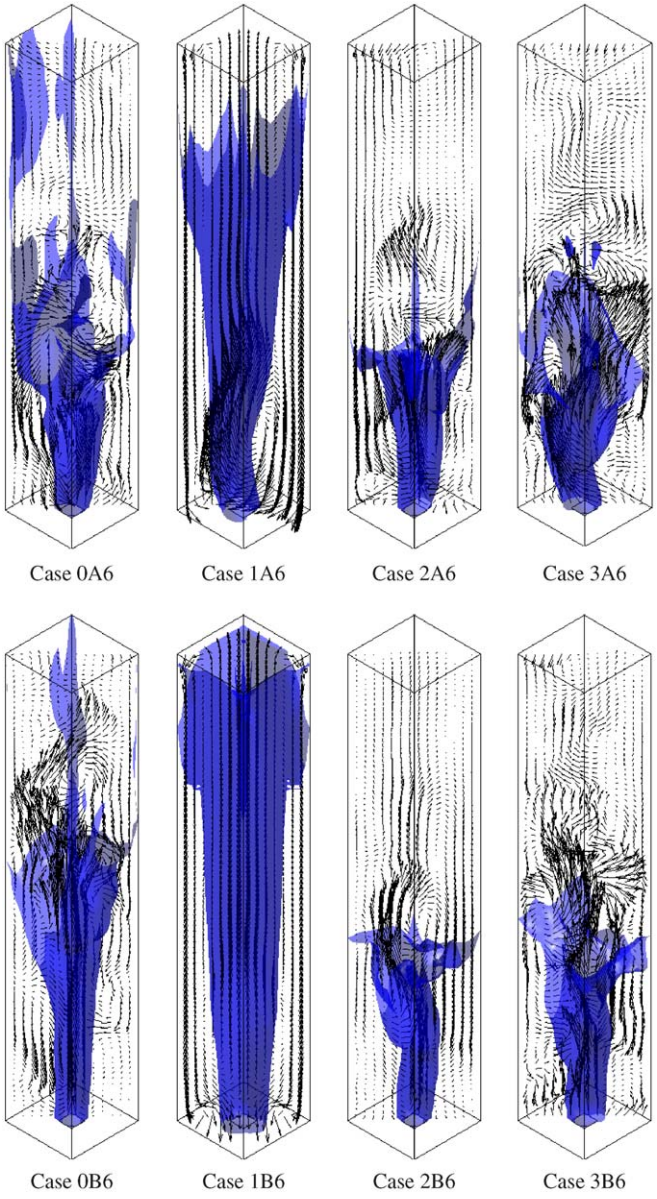

Fig. 10. Snapshots of the instantaneous iso-surface of $\alpha_G = 0.01$ and liquid velocity field after 500 s for different bubble-induced turbulence models and interfacial closure models.

Furthermore, it is found in Fig. 10 that compared to interfacial closure **A**, the interfacial models of Tomiyama increase the height where the bubble plume is spread throughout the cross section of the column. However, when Tomiyama's interfacial closures are adopted in the simulation of the lower column ($H/D = 3$), very steep vertical velocity profiles are found as shown in Fig. 11. In this case the large C_D and small C_L lead to a plume that is only meandering in the column centre, which is not in agreement with the experimental data. Combining the observations in Figs. 9–11, it is concluded that the spreading behavior of the bubble plume and therefore also the underlying interfacial closure model depends on the column aspect ratio.

In order to investigate the nature of the contradictory results obtained for different aspect ratios, some additional cases will be discussed in which only one of the interfacial forces was changed.

5.2.2. Tomiyama drag coefficients

Case 0A3 ($C_D = 0.98$), 0A3-TD ($C_D = 1.52$), 0A6 and 0A6-TD were employed to study the performance of the drag correlation proposed by Tomiyama (2004). In these cases all of the model parameters were identical except for the drag force closure model, which was varied for each of the cases. Fig. 12 provides a comparison of the simulated vertical velocity components from different drag models with the experimental data in two columns. In the lower column, the correlation of Ishii and Zuber (1979) gives better time-averaged vertical velocity profiles than the drag model of Tomiyama (2004), although, as can be deduced from Fig. 12, the slip velocity predicted by the latter model agrees better with the measured value (≈ 0.18 m/s).

From Fig. 12 it can be seen that as a result of the increase of C_D and the associated decrease in the slip velocity the gas hold-up is increased.

When the drag model of Tomiyama is used, the drag force between the gas and the liquid phase is increased. This force mainly works in the vertical direction. On the other hand, the force that is mainly responsible for the lateral spreading of the gas, i.e., the lift force, is not or only slightly affected by the change of C_D. The ratio of these two forces, i.e., the ratio of the drag force in the vertical direction to the lift force in the horizontal direction, roughly determines the amount of spreading of the bubble plume as a function of height. This explains why, as found in both columns, the predicted vertical velocity profiles are steeper when a higher drag coefficient is used. When comparing Fig. 12 with Figs. 9 and 11, it is concluded that the differences in bubble plume spreading behavior predicted by models **A** and **B** can only partially be attributed to the applied drag force model. Most of the observed differences are attributed to the lift force model.

Furthermore, as an increased drag force reduces the gas phase (bubble) velocity, the residence time of the gas phase increases, which directly leads to an increase of the gas hold up, as can be seen in Fig. 13.

5.2.3. Effect of the lift force

The effect of the lift force on the bubble column dynamics was studied for both columns through Case 0A3 ($C_L = 0.5$), 0A3-CLT (Tomiyama C_L), 0A6 and 0A6-CLT (see Table 3). In these cases only C_L was varied, whereas C_D and C_{VM} were kept constant. Fig. 14 provides the comparison of the simulated time-averaged vertical velocity and the experimental data. Clearly, the lift force has a significant impact on the velocity distribution: with the increase of the lift force the bubble plume becomes more dynamic leading to a decrease of the vertical velocity of both phases and subsequently to a flatter velocity profile. It appears that the results with $C_L = 0.5$ fit better with the experimental data in the lower column, while in the taller column, simulation results obtained with the lift closure of Tomiyama agree best with the measurements. This implies that the bubble plume spreading mechanism varies with the

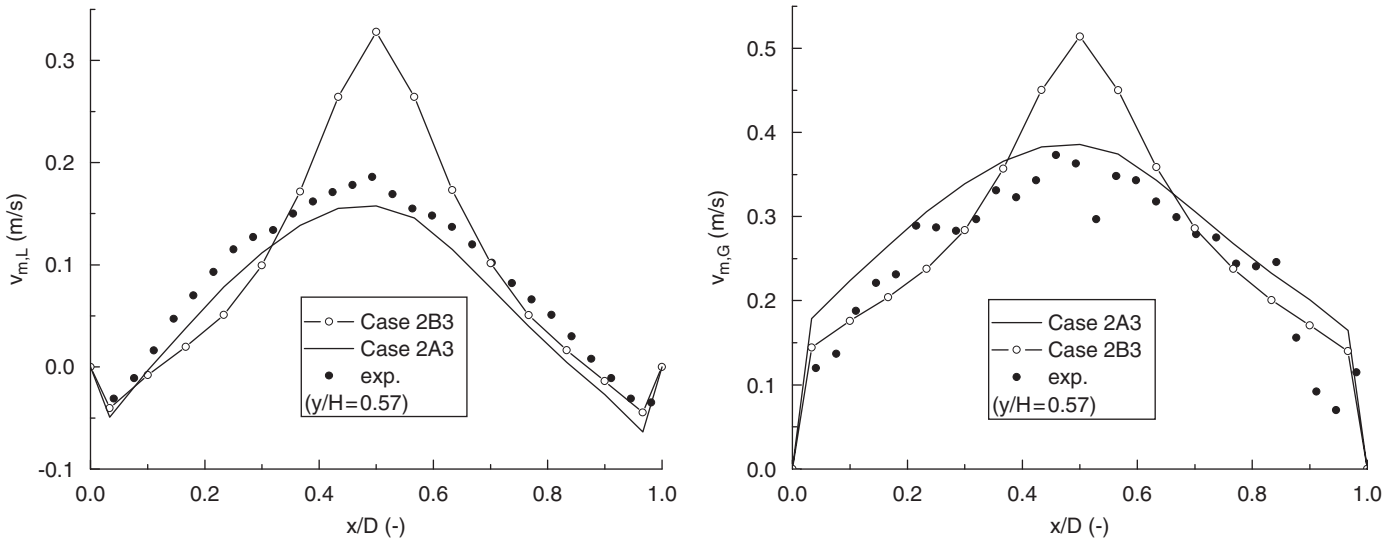

Fig. 11. Comparison of the simulated time-averaged vertical velocity profiles of both phases with the experimental data using different interfacial closures in a lower column.

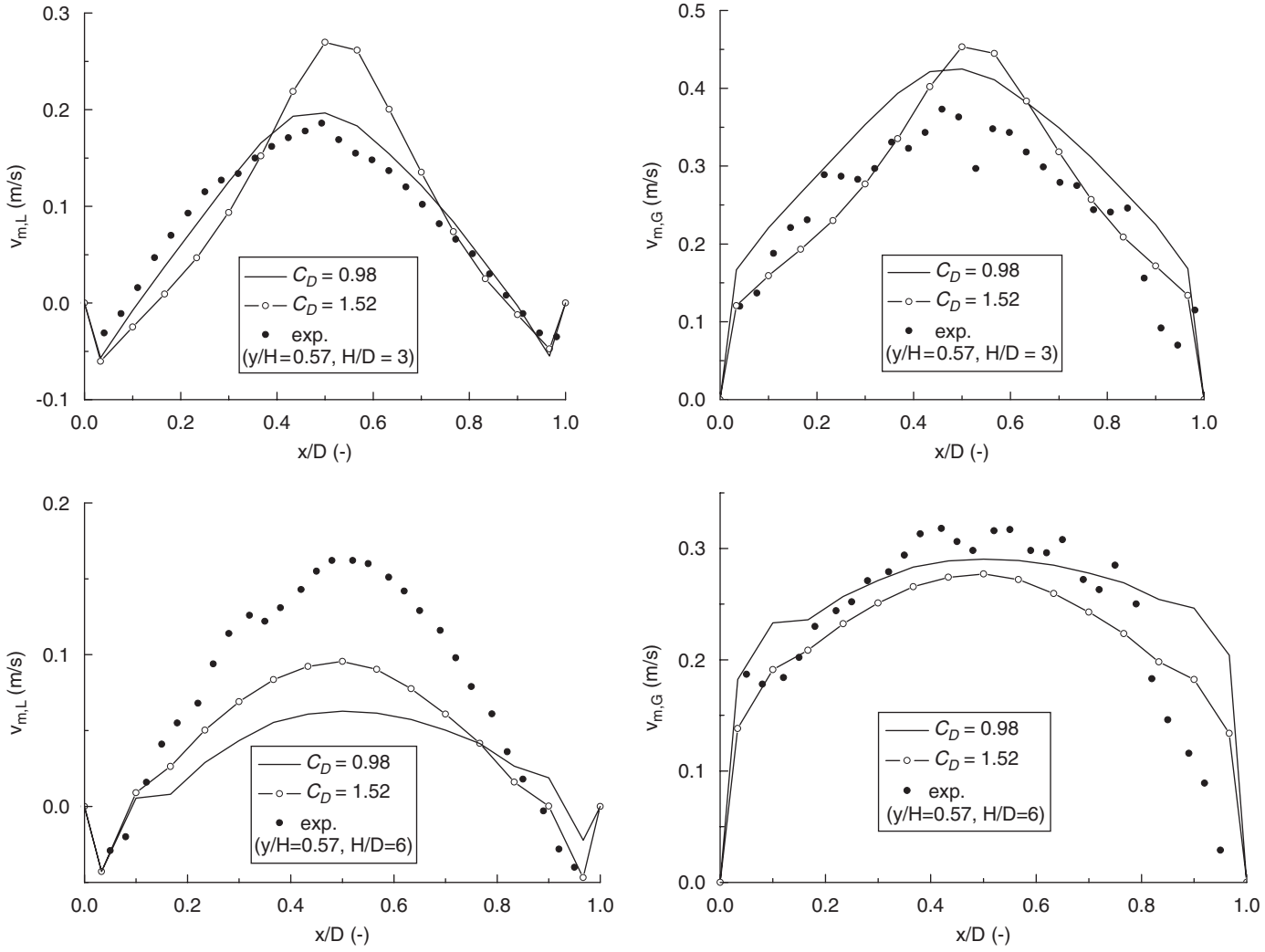

Fig. 12. Comparison of the time-averaged vertical velocity profiles obtained from two different drag models with experimental data of Deen et al. (2001) in two columns.

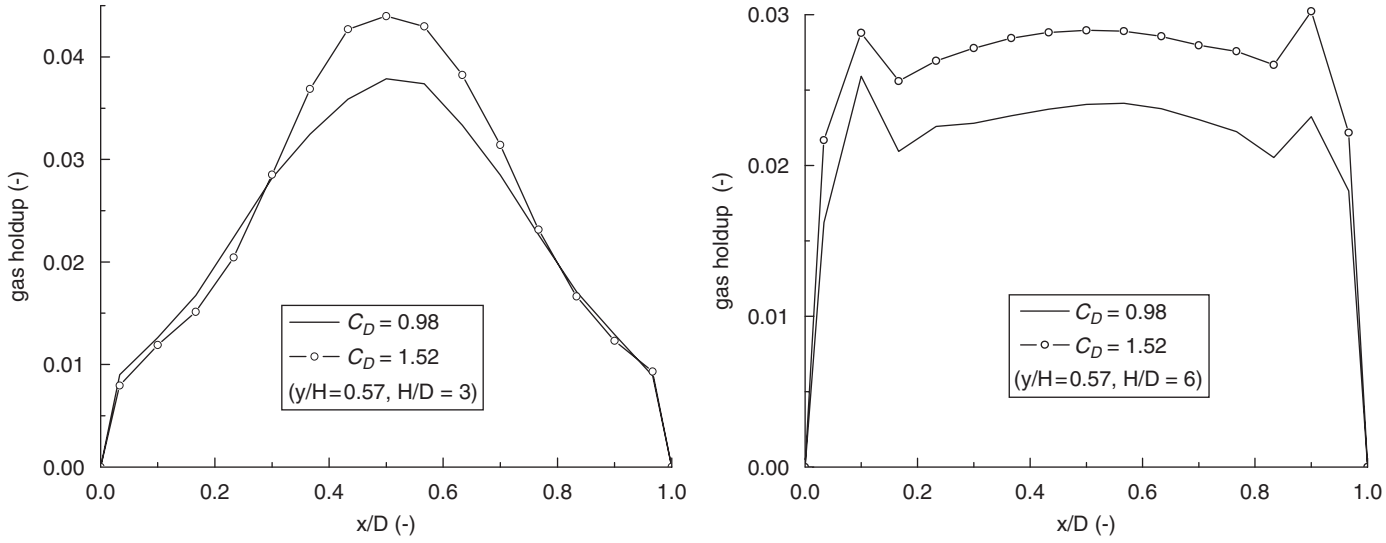

Fig. 13. Comparison of the simulated gas holdup profiles with different drag models in two columns.

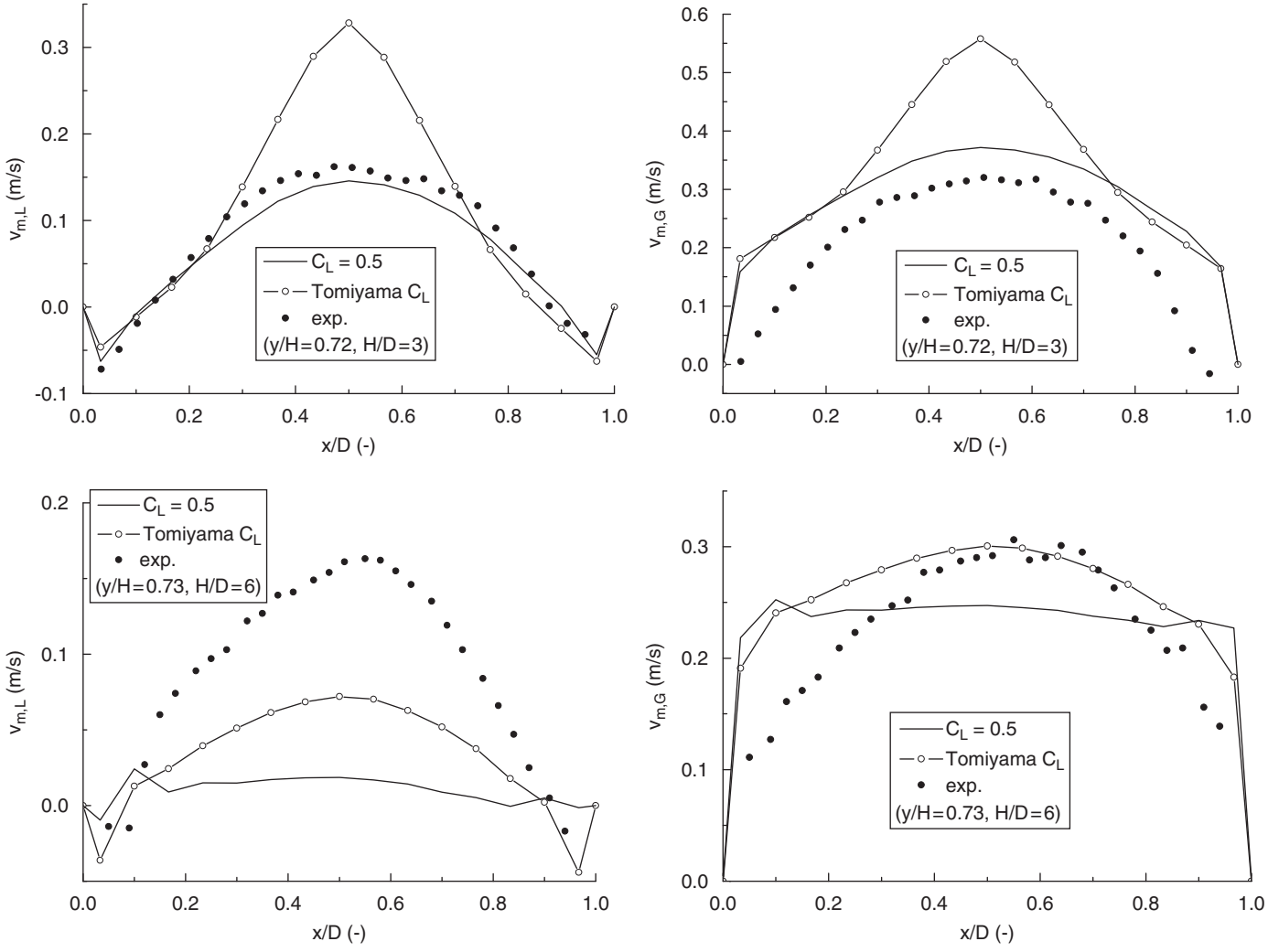

Fig. 14. Comparison of the time-averaged vertical velocity profile of the experimental data and those simulated with different C_L in two bubble columns.

column aspect ratio. As mentioned earlier, the ratio of the vertical drag force to the horizontal lift force roughly determines the amount of gas spreading. The lift coefficient of Tomiyama is approximately 0.29 in both columns; consequently, it leads to less spreading and a steeper vertical velocity distribution. Due to the reduced spreading of the plume the dynamics of

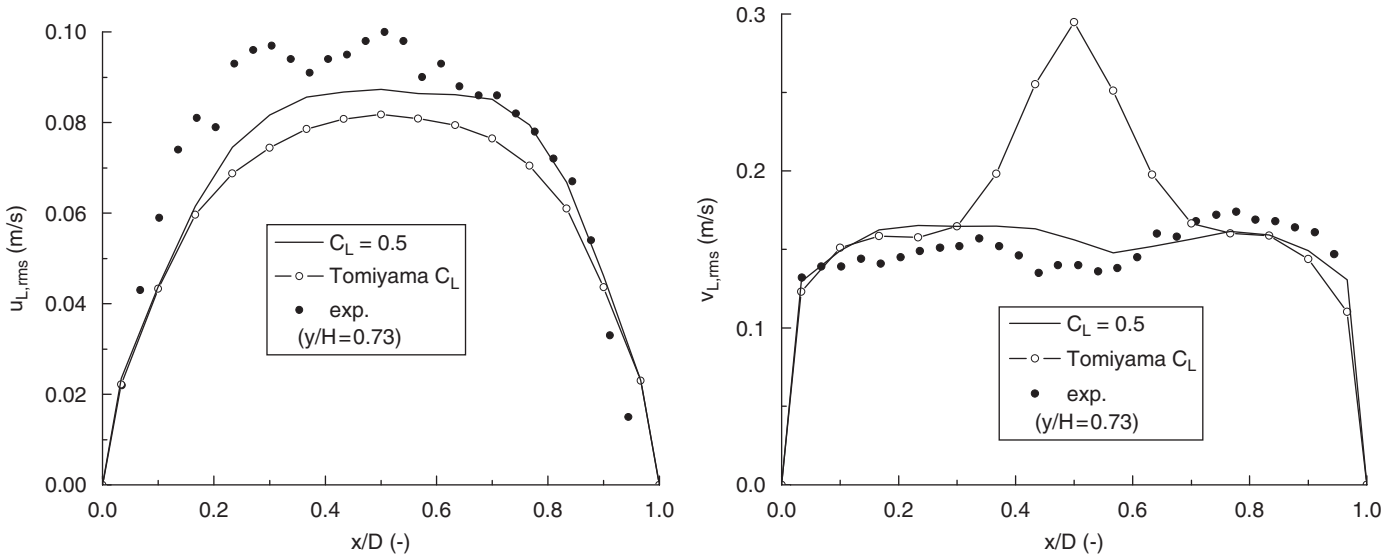

Fig. 15. Comparison of the simulated and experimental liquid velocity fluctuations for Case 0A3 and 0A3-CLT. Different C_L were used in the simulations.

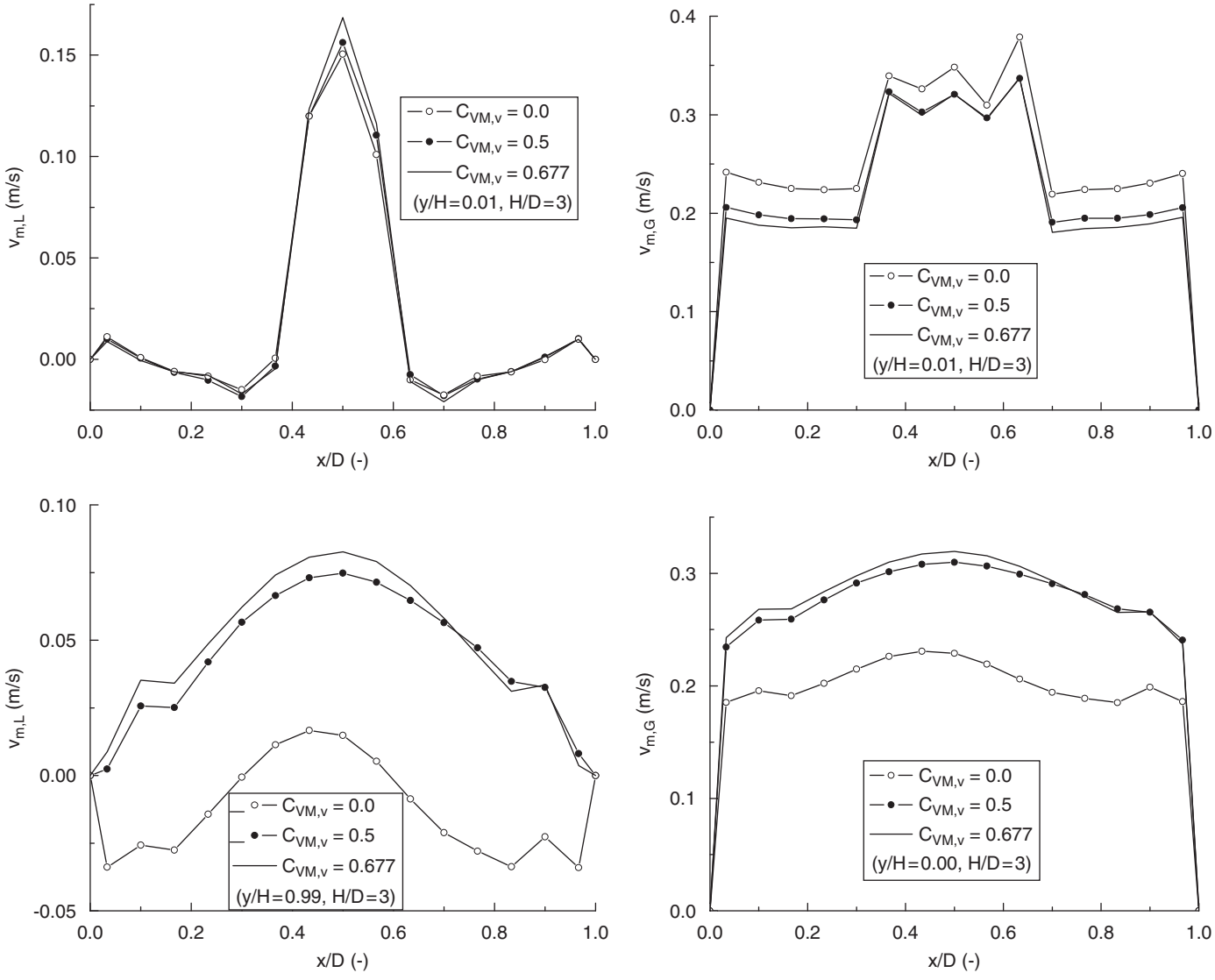

Fig. 16. Comparison of the simulated and experimental profiles of the vertical velocity. Different virtual mass coefficients were used in the simulation.

the plume are reduced. Consequently, as presented in Fig. 15, the velocity fluctuations in the horizontal direction are slightly reduced, whereas in the vertical direction, the velocity fluctuations are enhanced only in the column center where the bubble plume is present (see also Fig. 7). Though in the work of Pan et al. (1999) and Pfleger and Becker (2001), satisfactory results were obtained without lift force, a very steep velocity profile and quasi-steady bubble plume were observed in a numerical simulation with $C_L = 0$ conducted by the authors, which is in agreement with the findings of Deen et al. (2001). It is therefore concluded that the lift force plays a critical role in the prediction of the lateral behavior of the bubble plumes. Unfortunately, the different results for the two columns are not conclusive on the best lift closure. Possibly other aspects, such as the local gas fraction (hold-up effect) determine the exact value of the lift coefficient.

5.2.4. Effect of virtual mass force

The effect of the virtual mass force was investigated with the aid of Case 0A3, 0A3-VMT and 0A3-VM0, in which the vertical and horizontal virtual mass coefficients ($C_{VM,v}$, $C_{VM,h}$) are (0.5, 0.5), (0.68, 0.43) and (0, 0), respectively. Based on the work of Lopez de Bertodano (1992), the bubble relaxation time τ_{BIT} can be estimated to be about 0.006 s. So with an injected gas velocity of 0.1225 m/s, the acceleration distance is limited to about 1 mm. Therefore, comparisons of simulation results employing different virtual mass coefficients were made at the very bottom and top of the column, where the most important acceleration effects can be expected. Fig. 16 provides the comparisons among three simulated profiles of the mean vertical velocity of both phases at two heights. As shown in the figure, the virtual mass force suppresses the acceleration of the gas phase and increases the liquid velocity in the bottom part of the column, whereas at the very top of the column, it increases both the gas and liquid vertical velocities. From Fig. 16 as well as from the definition of the virtual mass force in Eq. (14), it is seen that the effect of the virtual mass force is to keep the slip velocity to be constant. At the bottom of the column, the differences among these three numerical results are quite small, which was also found in further comparisons at different heights. The influence of the virtual mass force on the flow is weak except at the very top of the column. The source of the differences observed in this region is not trivial, but may be attributed to the use of a pressure boundary condition at the top surface of the column. In reality the liquid bulk free surface is not a smooth plane as is assumed in the simulations, but a dynamic free surface. The larger discrepancies among the three cases at the top may be related to the present treatment of the outlet.

6. Conclusions

Numerical simulations of the gas–liquid two-phase flow in two squared-section bubble columns were conducted with the use of the commercial software package CFX-4.4. A sub-grid scale model and the k–ε model were employed to model the turbulent viscosity of the liquid phase. It was found that with increasing value of the sub-grid scale model constant C_S the turbulent viscosity increases, and consequently the mean velocity profiles become steeper, as the bubble plume dynamics are reduced. From this study, it is shown that with a value of $C_S = 0.08$–0.10, numerical results agree well with the experimental data. It is also found that the damping of the turbulent viscosity near the system walls is not inherently achieved with the SGS model of Smagorinsky in the simulation of bubbly flow, so in future work, the use of wall functions or another kind of SGS model should be considered.

For the k–ε model employing different approaches to model the shear-induced liquid phase turbulent viscosity, the differences between the three models to account for the bubble-induce turbulence was studied. The simulated liquid phase velocity fluctuations predicted with the models of Troshko and Hassan (2001) and Pfleger and Becker (2001) agree well with the measurements in the lower column. The model of Sato and Sekoguchi (1975) leads to a higher turbulent viscosity and only resolves the overall flow pattern, most of the transient details of the bubbly flow are implicitly contained in the sub-grid scale turbulence kinetic energy, k_L. As a consequence, a quasi-steady bubble plume behavior was predicted with this model. On the contrary, both the models of Pfleger and Becker (2001) and Troshko and Hassan (2001) can correctly reproduce dynamic bubble plume behavior.

For the chosen operating conditions, according to Lopez de Bertodano (1992), the characteristic time scale of the bubble-induced turbulence is about 0.006 s for both columns which is much smaller than the time scale of shear-induced turbulences (≈ 0.8 s for the standard k–ε model). The BIT model of Troshko and Hassan (2001) produces a near wall peak profile of the liquid phase effective viscosity, which is not very realistic.

Both the SGS and the k–ε turbulence models can produce a good solution for the time-averaged vertical velocity. When extra source terms are added in the equations of k and ε, not only the resolved velocity fluctuations agree with the measurements, the predicted bubble plume is as dynamic as that obtained from the SGS model, and additionally the mean and fluctuating velocities are in good agreement with the experimental observations. Based on all comparisons and findings, it can be concluded that for the cases studied in this work the k–ε model extended with the bubble-induced turbulence model of Pfleger and Becker (2001) and SGS model should be preferred for the simulation of bubbly flow.

Though simulated results obtained from Tomiyama's interfacial force closures do not satisfy the experimental data in the lower bubble column ($H/D=3$), in a taller column ($H/D=6$), Tomiyama's interfacial force closures produce a quite good solution. This observation implies that the way the bubble plume spreads over the whole column varies with the column aspect ratio and apparently there is not yet a universal interfacial closure model available for the simulation of bubbly flow. With a higher value for C_D and smaller value for C_L, Tomiyama's interfacial force closures increase the height where the bubble plume is spread out over the entire cross section of the column.

It was found that the closure model for the drag force strongly affects the vertical velocity profiles and the gas hold-up distri-

bution. In the lower column, the drag coefficient of Ishii and Zuber (1979) provides a better solution than that of Tomiyama (2004), though the latter model yields a better prediction of the slip velocity. In the taller column however, the drag correlation of Tomiyama produces a better solution than that of Ishii and Zuber. Both drag correlations are valid for the case of a single bubble; swarm effects on the drag force closure are not considered. Furthermore, as stated in the work of Tomiyama et al. (2002), the drag coefficient is also a function of the bubble aspect ratio. In the present work, the bubble aspect ratio was calculated according to Wellek et al. (1966). With an equivalent bubble diameter of 4 mm, recent front tracking results of Dijkhuizen et al. (2005) show that the bubble is considerably flatter, which has a significant influence on the drag coefficient. In future work, bubble aspect ratios based on front tracking simulation could be taken into account.

It was observed that the virtual mass force has a very small influence on the investigated bubbly flow as the zone at which the virtual mass force is active is quite small. The lift force on the contrary has a large impact on the flow dynamics, as it determines the dispersion of the bubble plume towards the bubble column walls and subsequently influences the shape of the vertical velocity profile. The lift coefficient of Tomiyama is preferred for the taller column. According to Tomiyama (2004), the lift coefficient depends on the bubble aspect ratio and local Reynolds number. As indicated earlier, it was found that the spreading mode of the plume varies with the column aspect ratio. This finding implies that the lift coefficient should also depend on the local gas hold-up and/or the local gradient of the gas hold-up.

In the present work, a pressure boundary condition is applied at the outlet. In reality, there is a gas cap, and the bulk water free surface is dynamic and not a smooth plane. Further work is still required to capture the bulk water free surface and obtain a good solution for the liquid phase velocity in the top portion of the column.

References

Becker, S., Sokolichin, A., Eigenberger, G., 1994. Gas–liquid flow in bubble columns and loop reactors: Part II. Comparison of detailed experiments and flow simulations. Chemical Engineering Science 49, 5747–5762.

Bel F'dhila, R., Simonin, O., 1992. Eulerian predictions of a turbulent bubbly flow downstream a sudden pipe expansion. In: Sommerfeld, M. (Ed.), Sixth Workshop on Two-Phase Flow Predictions. Erlangen, Germany.

Borchers, O., Busch, C., Eigenberger, G., 1999. Applicability of the standard k-e turbulence model to the dynamic simulation of bubble columns Part II: comparison of detailed experiments and the simulations. Chemical Engineering Science 54, 5927–5935.

Canuto, V.M., Cheng, Y., 1997. Determination of the Smagorinsky–Lilly constant. Physics of Fluids 9, 1368–1378.

Clift, R., Grace, J.R., Weber, M.E., 1978. Bubbles, Drops and Particles. Academic Press, New York.

Darmana, D., Deen, N.G., Kuipers, J.A.M., 2005. Detailed modeling of hydrodynamics, mass transfer and chemical reactions in a bubble column using a discrete bubble model. Chemical Engineering Science 60, 3383–3404.

Darmana, D., Deen, N.G., Kuipers, J.A.M., 2006. Parallelization of an Euler–Lagrange model using mixed domain decomposition and a mirror domain technique: application to dispersed gas–liquid two-phase flow. Journal of Computational Physics, accepted for publication.

Deen, N.G., 2001. An experimental and computational study of fluid dynamics in gas–liquid chemical reactors. Ph.D. Thesis, Aalborg University, Esbjerg, Denmark.

Deen, N.G., Solberg, T., Hjertager, B.H., 2001. Large eddy simulation of the gas–liquid flow in a square cross-sectioned bubble column. Chemical Engineering Science 56, 6341–6349.

Delnoij, E., Kuipers, J.A.M., Van Swaaij, W.P.M., 1997. Dynamic simulation of gas–liquid two-phase flow: effect of column aspect ratio on the flow structure. Chemical Engineering Science 52, 3759–3772.

Dijkhuizen, W., Van den Hengel, E.I.V., Deen, N.G., van Sint Annaland, M., Kuipers, J.A.M., 2005. Numerical investigation of closures for interface forces acting on single air-bubbles in water using volume of fluid and front tracking models. Chemical Engineering Science 60, 6169–6175.

Drew, D. A., Passman, S. L., 1999. Theory of multicomponent fluids. Applied Mathematical Sciences 135.

Ervin, E.A., Tryggvason, G., 1997. The rise of bubbles in a vertical shear flow. Journal of Fluids Engineering 119, 443–449.

Gosman, A.D., Issa, R.I., Lekakou, C., Looney, M.K., Politis, S., 1992. Multidimensional modeling of turbulent two-phase flows in stirred vessels. A.I.Ch.E. Journal 38, 1946–1955.

Ishii, M., Zuber, N., 1979. Drag coefficient and relative velocity in bubbly, droplet or particulate flows. A.I.Ch.E. Journal 25, 843–855.

Jakobsen, H.A., Sannæs, B.H., Grevskott, S., Svendsen, H.F., 1997. Modeling of vertical bubble-driven flows. Industrial Engineering Chemistry and Research 36, 4052–4074.

Kataoka, I., Serizawa, A., 1989. Basic equations of turbulence in gas–liquid two-phase flow. International Journal of Multiphase Flow 15, 843–855.

Lakehal, D., Smith, B.L., Milelli, M., 2002. Large-eddy simulation of bubbly turbulent shear flows. Journal of Turbulence 3, 1–21.

Lopez de Bertodano, M.A., 1992. Turbulent bubbly two-phase flow in a triangular duct. Ph.D. Dissertation, Rensselaer Polytechnic Institute.

Lopez de Bertodano, M.A., Lahey, R.T., Jones, O.C., 1994. Development of a k–ε model for bubbly two-phase flow. Journal of Fluids Engineering 116, 128–134.

Magnaudet, J., Eames, I., 2000. The motion of high-Reynolds number bubbles in inhomogeneous flows. Annual Review of Fluid Mechanics 32, 659–708.

Milelli, M., Smith, B.L., Lakehal, D., 2001. Large-eddy simulation of turbulent shear flows laden with bubbles. In: Geurts, B.J., Friedrich, R., Metais, O. (Eds.), Direct and Large-Eddy Simulation IV. Kluwer Academic Publishers, Amsterdam, pp. 461–470.

Mudde, R.F., Simonin, O., 1999. Two- and three dimensional simulations of a bubble plume using a two-fluid model. Chemical Engineering Science 54, 5061–5069.

Oey, R.S., Mudde, R.F., Van Den Akker, H.E.A., 2003. Sensitivity study on interfacial closure laws in two-fluid bubbly flow simulations. A.I.Ch.E. Journal 49, 1621–1636.

Pan, Y., Dudukovic, M.P., Chang, M., 1999. Dynamic simulation of bubbly flow in bubble columns. Chemical Engineering Science 54, 2481–2489.

Pfleger, D., Becker, S., 2001. Modeling and simulation of the dynamic flow behavior in a bubble column. Chemical Engineering Science 56, 1737–1747.

Sato, Y., Sekoguchi, K., 1975. Liquid velocity distribution in two-phase bubble flow. International Journal of Multiphase Flow 2, 79–95.

Smagorinsky, J., 1963. General circulation experiments with the primitive equations. Monthly Weather Review 91, 99–165.

Sokolichin, A., Eigenberger, G., 1999. Applicability of the standard turbulence model to the dynamic simulation of bubble columns: Part I. Detailed numerical simulations. Chemical Engineering Science 52, 611–626.

Sokolichin, A., Eigenberger, G., Lapin, A., 2005. Simulation of buoyancy driven bubbly flow: established simplifications and open questions. A.I.Ch.E. Journal 50, 24–45.

Svendsen, H.F., Jakobsen, H.A., Torvik, R., 1992. Local flow structures in internal loop and bubble column reactors. Chemical Engineering Science 47, 3297–3304.

Tomiyama, A., 1998. Struggle with computational bubble dynamics. Third International Conference on Multiphase Flow, ICMF, Lyon, France.

Tomiyama, A., 2004. Drag lift and virtual mass forces acting on a single bubble. Third International Symposium on Two-Phase Flow Modeling and Experimentation, Pisa, Italy, 22–24 September.

Tomiyama, A., Sou, A., Zun, I., Kanami, N., Sakaguchi, T., 1995. Effect of Eötvös number and dimensionless liquid volumetric flux on lateral motion of a bubble in a laminar duct flow. In: Proceedings of the Second International Conference on Multiphase Flow. Kyoto, Japan.

Tomiyama, A., Celata, G.P., Hosokawa, S., Yoshida, S., 2002. Terminal velocity of single bubbles in surface tension force dominant regime. International Journal of Multiphase Flow 28, 1497–1519.

Torvik, R., Svendsen, H.F., 1990. Modelling of slurry reactors. A fundamental approach. Chemical Engineering Science 45, 2325–2332.

Troshko, A.A., Hassan, Y.A., 2001. A two-equation turbulence model of turbulent bubbly flows. International Journal of Multiphase Flow 27, 1965–2000.

Van den Hengel, E.I.V., Deen, N.G., Kuipers, J.A.M., 2005. Application of coalescence and breakup models in a discrete bubble model for bubble columns. Industrial Engineering Chemistry and Research 44, 5233–5245.

Van Driest, E.R., 1956. On the turbulent flow near a wall. Journal of Aeronautical Science 23, 1007–1011.

Viollet, P.L., Simonin, O., 1994. Modeling dispersed two-phase flows: closure, validation and software development. Applied Mechanical Reviews 47, S80.

Vreman, A.W., 2004. An eddy-viscosity subgrid-scale model for turbulent shear flow: algebraic theory and applications. Physics of Fluids 16, 3670–3681.

Wellek, R.M., Agrawal, A.K., Skelland, A.H.P., 1966. Shape of liquid drops moving in liquid media. A.I.Ch.E. Journal 12, 854–862.

Zhang, D., Deen, N.G., Kuipers, J.A.M., 2005. Numerical simulation of dynamic flow behavior in a bubble column: comparison of the bubble-induced turbulence models in the k–ε model. Fourth International Conference on CFD in the Oil and Gas, Metallurgical & Process Industries, Trondheim, Norway, 6–8 June 2005.